Resonance Energy Transfer in a Model System of Membranes: Application to Gel and Liquid Crystalline Phases

Luís M. S. Loura, Aleksandre Fedorov and Manuel Prieto
Centro de Química-Física Molecular, Complexo I, Instituto Superior Técnico, 1096 Lisboa Codex, Portugal

ABSTRACT Resonance energy transfer between octadecyl rhodamine B (donor) and 1,1',3,3,3',3'-hexamethylindotricarbocyanine (acceptor) was studied in a model system of membranes (large unilamellar vesicles of dipalmitoylphosphatidylcholine), using both steady-state and time-resolved techniques. In the fluid phase (temperature = 50°C) the decay law and the steady-state theoretical curve for energy transfer in two dimensions are verified. In the gel phase (temperature = 25°C) an apparent reduction of dimensionality is observed, which is explained on the basis of probe segregation to the defect lines (grain boundaries). An estimation of the domain size from the model recovered linear probe concentrations is approximately 1750–2000 lipid molecules. In both phases, the existence of a fractal geometry was ruled out.

INTRODUCTION

Lipid self-organization in membranes is a relevant problem in biophysics. Because of their complexity, biological membranes are often replaced by model systems, such as phospholipid vesicles, which are formed by single or multiple bilayers dispersed in aqueous medium. On variation of temperature or pressure, the lipid undergoes structural changes related to phase transitions. Bilayers of all lipids show a first-order transition (associated with melting of the alkyl chains) from the so-called $L_{\beta'}$ gel phase to the fluid L_α phase. In large excess of water, there is an additional phase transition, called the pretransition, from $L_{\beta'}$ to the "ripple phase" $P_{\beta'}$ (Sackmann, 1982).

Lateral lipid organization (e.g., domain formation) is supposed to modulate biochemical processes such as protein function (Heimburg and Biltonen, 1996). The lipid phases were shown to be considerably different when freeze-etched samples are observed by electron microscopy, which is useful to characterize domains with sizes >0.1 μm (Sackmann, 1982). The $L_{\beta'}$ phase generally shows a surface with defect lines, the $P_{\beta'}$ phase shows a wavelike surface profile and the L_α phase exhibits a completely smooth surface.

Other techniques have been used to study the nature and extent of lipid aggregation, including fluorescence microscopy (limiting resolution 0.5 μm; e.g., Parasassi et al., 1994), calorimetry (useful to measure the nonideality of binary mixtures; e.g., Mabrey and Sturtevant, 1976) and fluorescence recovery after photobleaching (for studying percolation in gel-fluid coexistence regions, e.g., Almeida et al., 1992, and determination of diffusion coefficients, e.g., Derzko and Jacobson, 1980). However, these techniques do not give information about domains in the 10- to 100-nm size range. Indirect characterization has been achieved using electron spin resonance spectroscopy (Sankaram et al., 1992) and infra-red spectroscopy (Mendelsohn et al., 1995; Snyder et al., 1995) in binary lipid mixtures. In the former study, the number of molecules per lipid domain was determined for several compositions. For the fluid phase domains, values of up to 1000 molecules (depending on the fluid phase fraction) were reported. For the gel phase domain, this number increases approximately twofold. The infra-red method is sensitive to domain sizes between 1–100 molecules.

In this work, ET will be used to probe lipid lateral organization in gel and fluid phases. The range of this interaction (~100 Å) is adequate to probe small size domains. In addition, because of its explicit distance dependence (energy transfer rate being proportional to r^{-6}), detailed information on distance distribution functions and/or the dimensionality of the system can be obtained. The used Förster pair was ORB as donor and $DiIC_1(7)$ as acceptor, these probes being incorporated in LUV of DPPC, above and below the main phase transition temperature (T_m = 41.4 ± 0.5°C) (Marsh, 1990). In addition, a steady-state study of energy migration among ORB molecules was also carried out to obtain independent information on its distribution function.

THEORETICAL BACKGROUND

ET in heterogeneous media

Since the formulation of the fluorescence decay functions in 1D and 2D in the mid-1970s (Hauser et al., 1976) and its extension to systems with self-similar structure in the mid-1980s (Klafter and Blumen, 1984), Förster type ET in

Received for publication 25 March 1996 and in final form 24 June 1996.

Abbreviations used: 1D, one-dimensional; 2D, two-dimensional; $DiIC_1(7)$, 1,1',3,3,3',3'-hexamethylindotricarbocyanine; DPPC, dipalmitoylphosphatidylcholine; ET, resonance energy transfer; LUV, large unilamellar vesicles; NBD, *N*-(7-nitrobenz-2-oxa-1,3-diazol-4-yl); ORB, octadecyl rhodamine B; χ^2_G, global χ^2 value.

Address reprint requests to Dr. Manuel José Estevez Prieto, Centro de Quimica Fisica Molecular, Instituto Superior Tecnico, Av. Rovisco Pais, 1096 Lisboa Codex, Portugal. Tel.: 351-1-8419219; Fax: 351-1-3524372; E-mail: prieto@alfa.ist.utl.pt.

Dr. Fedorov is on leave from Vavilov Optical State Institute, St. Petersburg, Russia.

0006-3495/96/10/1823/14 $2.00

restricted arrangements has attracted the interest of many researchers. Studies involving such diverse media as silica surfaces (Rojanski et al., 1986), porous glasses (Even et al., 1984), polymer interphases (Farinha et al., 1995), Langmuir-Blodgett films (Yamazaki et al., 1987; Ohta et al., 1993), and vesicles (Tamai et al., 1987; Duportail et al., 1995) have been reported, and ET is now established as a powerful tool for obtaining structural information concerning these systems.

Fluorescence decays were usually analyzed using Eq. 1 (Klafter and Blumen, 1984),

$$i_{DA}(t) = A \cdot \exp(-t/\tau - C\,(t/\tau)^{d/6}) \quad (1)$$

where $i_{DA}(t)$ is the time-resolved donor fluorescence intensity in the presence of acceptor, A is a constant, τ is the donor fluorescence lifetime in the absence of acceptor, and d is the dimensionality of the system. For the Euclidean dimensionalities, the C factor is given by Eq. 2 (Hauser et al., 1976),

$$C = \Gamma(1 - d/6) \cdot n_{dA} \cdot V_d \cdot R_0^d \quad (2)$$

Γ is the complete gamma function, n_{dA} the number of acceptors per d-space volume unit (e.g., n_{2A} is the number of acceptors per area unit), V_d is the d-dimensional unit sphere ($V_1 = 2$, $V_2 = \pi$, $V_3 = 4\pi/3$), and R_0 is the critical Förster radius. Noninteger d values were usually interpreted on the basis of a fractal structure. However, as first pointed out by Yang et al. (1985) and Klafter and Blumen (1985), an "apparent fractal" dimension may not be due to an actual self-similar structure, but to restricted dimensions of the medium (i.e., nonvalidity of the "infinite medium" assumption). Several theoretical and experimental confirmations of this fact have appeared since then (Blumen et al., 1986; Levitz and Drake, 1987; Levitz et al., 1988; Pekcan et al., 1990). Another major source of deviation from integer dimensionality, perhaps even more important than the former, may stem from nonrandom distribution of acceptors (contrary to the assumptions made in the deduction of Eq. 1). Again in this case, and because of the ability of the stretched exponential decay function (Eq. 1, with generally noninteger d) to analyze most decay data (even when there is no physical evidence for noninteger dimensionality), fractal structure was often mistakenly invoked.

Time-resolved model fitting methodology

The time-resolved ET experiment consists of obtaining several fluorescence decay curves for different acceptor concentrations. Until recently, each decay within the same experiment was analyzed separately, τ being sometimes fixed to the value recovered in the absence of acceptor. An alternative procedure is the use of global analysis (for a review, see Beechem et al., 1991). In this method, all related decays are analyzed simultaneously and the common parameters (τ and d in Eq. 1) are linked through the various curves. Instead of several optimizing functions (one χ^2 value for each decay), there is a single χ^2 (the global χ^2) value for the whole experiment. It has been found that, for the accurate recovery of complex fluorescence decay phenomena parameters, it is advantageous to combine more than one experiment into the analysis (as first shown by Eisenfeld and Ford, 1979). The use of a smaller number of total fit parameters provides a more critical test of the model. Global analysis has been successfully used in many situations, including two-state excited-state reactions, anisotropy decay data analysis and distributions of distances through ET (Beechem et al., 1991). The application of global analysis to ET to an ensemble of acceptors in restricted media is, however, more recent (Maliwal et al., 1995; Ballet et al., 1996).

The fluorescence decay of a probe in a heterogeneous medium is sometimes intrinsically complex, i.e., nonmonoexponential (Maliwal et al., 1995; Ballet et al., 1996). If it can be described by the sum of two exponentials, Eq. 3,

$$i_D(t) = A_1 \cdot \exp(-t/\tau_1) + A_2 \cdot \exp(-t/\tau_2) \quad (3)$$

then Eq. 1 should be reformulated as

$$i_{DA}(t) = A_1 \cdot \exp(-t/\tau_1 - C_1 \cdot (t/\tau_1)^{d/6}) + A_2 \cdot \exp(-t/\tau_2 - C_2 \cdot (t/\tau_2)^{d/6}) \quad (4)$$

If Eq. 4 were used for analyzing decay data, the C_1 and C_2 parameters would be allowed to assume totally independent values. Under reasonable physical assumptions, an additional simplification can be introduced. Those parameters are related to the Förster radius, Eq. 5 (see Eq. 2):

$$C_i = \alpha \cdot R_{0i}^d \quad i = 1, 2 \quad (5)$$

where α depends only on dimensionality. R_{0i} denotes the critical Förster radius associated to each lifetime component. If the two donor populations have identical fluorescence spectra but different fluorescence quantum yields Φ_{Di}, then we should have (see Materials and Methods):

$$R_{0i} = \beta \cdot \Phi_{Di}^{1/6} \quad i = 1, 2 \quad (6)$$

Φ_{Di} can be related to each lifetime by

$$\Phi_{Di} = k_{Fi} \cdot \tau_i \quad (7)$$

where k_{Fi} is the fluorescence emission rate constant for population i. In case that the oscillator strength is identical for the two species, $k_{F1} = k_{F2} = k_F$. Eq. 8 then holds,

$$R_{0i} = \gamma \cdot \tau_i^{1/6} \quad (8)$$

with $\gamma = \beta \cdot k_F^{1/6}$, and after substitution in Eq. 5:

$$C_i = c \cdot \tau_i^{d/6} \quad (9)$$

where $c = \alpha \cdot \gamma^d$. Eq. 4 can then be rewritten as

$$i_{DA}(t) = A_1 \cdot \exp(-t/\tau_1 - c \cdot t^{d/6}) + A_2 \cdot \exp(-t/\tau_2 - c \cdot t^{d/6}) \quad (10)$$

where a single parameter c is considered.

This is the fitting equation used for a single-curve analysis. For global analysis of several decays, four parameters should be linked throughout the whole set of experimental curves, the two lifetimes τ_1 and τ_2, the dimensionality d, and the ratio of preexponential factors $Q = A_1/A_2$. For each curve, there are two additional decay parameters, one preexponential factor (A_1 or A_2) and c. We have also considered a scatter coefficient (sc) to take into account light-scattering artifacts according to (O'Connor and Philips, 1984):

$$F_{DA}(t) = L(t)*i_{DA}(t) + sc \cdot L(t) \tag{11}$$

where $F_{DA}(t)$ is the experimental decay curve (not deconvoluted), $L(t)$ is the instrumental response function and * stands for convolution (in our results, we always had $sc \ll A_i$).

In summary, for a set of j curves, the maximum number of fitting parameters is $4 + 3j$, although, in practice, the number of fluctuating parameters is $3 + 3j$, because c is fixed at zero for the system with no acceptor. The linked parameters are τ_1, τ_2, d, and Q.

When dealing with heterogeneous systems on experimental grounds, one often has to include an additional term, representing donor molecules that are not affected by acceptors, to recover acceptable fits to the decay data (Yamazaki et al., 1987; Ohta et al., 1993; Ballet et al., 1996). Eq. 1 then becomes

$$i_{DA}(t) = A \cdot \exp(-t/\tau - C \cdot (t/\tau)^{d/6}) + r \cdot A \cdot \exp(-t/\tau) \tag{12}$$

for a single-lifetime-decaying donor, and Eq. 10 is now written as

$$\begin{aligned} i_{DA}(t) = {} & A_1 \cdot \exp(-t/\tau_1 - c \cdot t^{d/6}) \\ & + A_2 \cdot \exp(-t/\tau_2 - c \cdot t^{d/6}) \\ & + r \cdot (A_1 \cdot \exp(-t/\tau_1) + A_2 \cdot \exp(-t/\tau_2)) \end{aligned} \tag{13}$$

where r denotes the ratio of donors unaffected by acceptors to those that are involved in energy transfer. The number of fluctuating parameters would now be $2 + 4j$ (note that r is fixed at zero for the system with no acceptor).

Steady-state ET formalism

Independent experimental information can be obtained through steady-state measurements. In the absence of static quenching, the function that relates the steady-state fluorescence intensity in the presence of acceptor (I_{DA}) to the acceptor concentration is readily obtained by integration of the decay laws,

$$I_{DA}/I_D = \int_0^\infty i_{DA}(t)dt \Big/ \int_0^\infty i_D(t)dt \tag{14}$$

where I_D is the steady-state fluorescence intensity in the absence of acceptor. Wolber and Hudson (1979) performed this integration analytically for 2D geometry:

$$I_{DA}/I_D = \sum_{j=0}^{\infty}(-\pi \cdot \Gamma(2/3) \cdot R_0^2 \cdot n_{2A})^j \cdot \Gamma(j/3 + 1)/j! \tag{15}$$

In the derivation of Eq. 15 it is assumed that the exclusion distance, L (minimum distance between donor and acceptor molecules), is much smaller than R_0. If this is not the case, more cumbersome exact expressions for I_{DA}/I_D (including an exclusion parameter) can be used. A different approach, using Monte Carlo simulations, was conducted by Snyder and Freire (1982). These authors adjusted practical polynomials to their results, and their fitting functions are used in this work. For $R_0/L > 4$, the exclusion parameter effect on the quenching curve is negligible. For 1D ET geometry, we obtained from analytical integration:

$$I_{DA}/I_D = \sum_{j=0}^{\infty}(-2 \cdot \Gamma(5/6) \cdot R_0 \cdot n_{1A})^j \cdot \Gamma(j/6 + 1)/j! \tag{16}$$

Energy migration (homotransfer)

In addition to the heterogeneous ET measurements, we also carried out a study of energy migration among donor molecules to obtain independent information on its intrinsic distribution function. The observable measured was the steady-state fluorescence anisotropy $\langle r \rangle$, namely its decrease on increasing probe concentration.

For 2D geometry, the Snyder and Freire (1982) Monte Carlo approach was used (see Table 1 of their work). For 1D geometry there is not such a practical formalism available. In any case, $\langle r \rangle$ can still be calculated from the integrated emission components' decay functions,

$$\langle r \rangle = \left(\int_0^\infty I_{VV}(t)dt - \int_0^\infty I_{VH}(t)dt\right) \Big/ \left(\int_0^\infty I_{VV}(t)dt + 2 \cdot \int_0^\infty I_{VH}(t)dt\right) \tag{17}$$

where the different intensities are the time-resolved vertical and horizontal components of the fluorescence emission ($I_{VV}(t)$ and $I_{VH}(t)$, respectively) with excitation vertical to the emission axis.

For concentrated samples, a loss of polarization (decrease in $\langle r \rangle$) is often observed. This concentration depolarization is caused by ET between alike (donor) molecules (energy migration; e.g., see Sienicki et al., 1989, and references therein). Under simplifying assumptions, the following set of equations applies:

$$I_{VV}(t) = \rho(t) \cdot [1 + 0.8 \cdot G^s(t)] \quad (18)$$

$$I_{VH}(t) = \rho(t) \cdot [1 - 0.4 \cdot G^s(t)] \quad (19)$$

In these equations, $\rho(t)$ is the isotropic decay function, and $G^s(t)$ is the ensemble averaged probability that an originally excited donor is still excited after time t. This function can be evaluated for integer dimensionality in a relatively simple manner, using the two-particle model for donor-donor migration (Baumann and Fayer, 1986):

$$G^s(t) = \exp[-2^{d/6-1} \cdot \Gamma(1 - d/6) \cdot n_{dD} \cdot V_d \cdot R_0^d \cdot (t/\tau)^{d/6}] \quad (20d)$$

where n_{dD} is the number of donors per d-space volume unit, and R_0 is now the donor-donor Förster radius.

For calculation of $\langle r \rangle$, one may calculate $I_{VV}(t)$ and $I_{VH}(t)$ by numerical integration (or analytical integration, solutions in this case being identical to the heterotransfer ones, minus the $2^{d/6-1}$ factor) of Eqs. 18 and 19, respectively, and then substitute the obtained values in Eq. 17. This was the procedure used for calculating 1D concentration depolarization curves. For $d = 2$, the Snyder and Freire (1982) formalism has the advantage of including a possibility of return of the excitation to the originally excited donor molecule from all other donors, instead of excluding all return paths requiring more than two molecules, as in the two-particle model. However, for moderately dilute samples, the two-particle model values are very close to those obtained with more complicated approaches (Sienicki et al., 1989).

MATERIALS AND METHODS

Experimental

In our experiment, ORB was used as donor and $DiIC_1(7)$ was used as acceptor (structures depicted in Fig. 1). Both probes were purchased from Molecular Probes (Eugene, OR) and used without further purification. DPPC was obtained from Avanti Polar Lipids (Birmingham, AL) and used as received. LUV of DPPC (ca. 1 mM) in buffer (Tris-HCl 50 mM, NaCl 50 mM, ethylenediaminetetraacetic acid 0.2 mM, pH = 7.4) were prepared as described elsewhere (Prieto et al., 1994). Adequate volumes of donor and acceptor solutions in methanol were added to the lipid dispersions. Incorporation of both probes (monitored from fluorescence intensity) was complete in 1 hr. The ratio ORB:DPPC was ~1:10,000, so that donor excitation energy migration in the heterotransfer experiments is negligible (Johansson and Niemi, 1987). The $DiIC_1(7)$:DPPC ratio was varied between 1:900 and 1:160. In the homotransfer study, the same lipidic systems were used, and the ORB:DPPC ratio was varied between 1:1800 and 1:300. The final lipid concentration was determined by phosphorus analysis (McClare, 1971). Probe concentrations were calculated using molar absorption coefficients in ethanol ϵ(ORB, 555 nm) = 85×10^3 $M^{-1}\cdot cm^{-1}$ (Johansson and Niemi, 1987) and $\epsilon(DiIC_1(7), 741\ nm) = 215\times10^3$ $M^{-1}\cdot cm^{-1}$ (Brackmann, 1986).

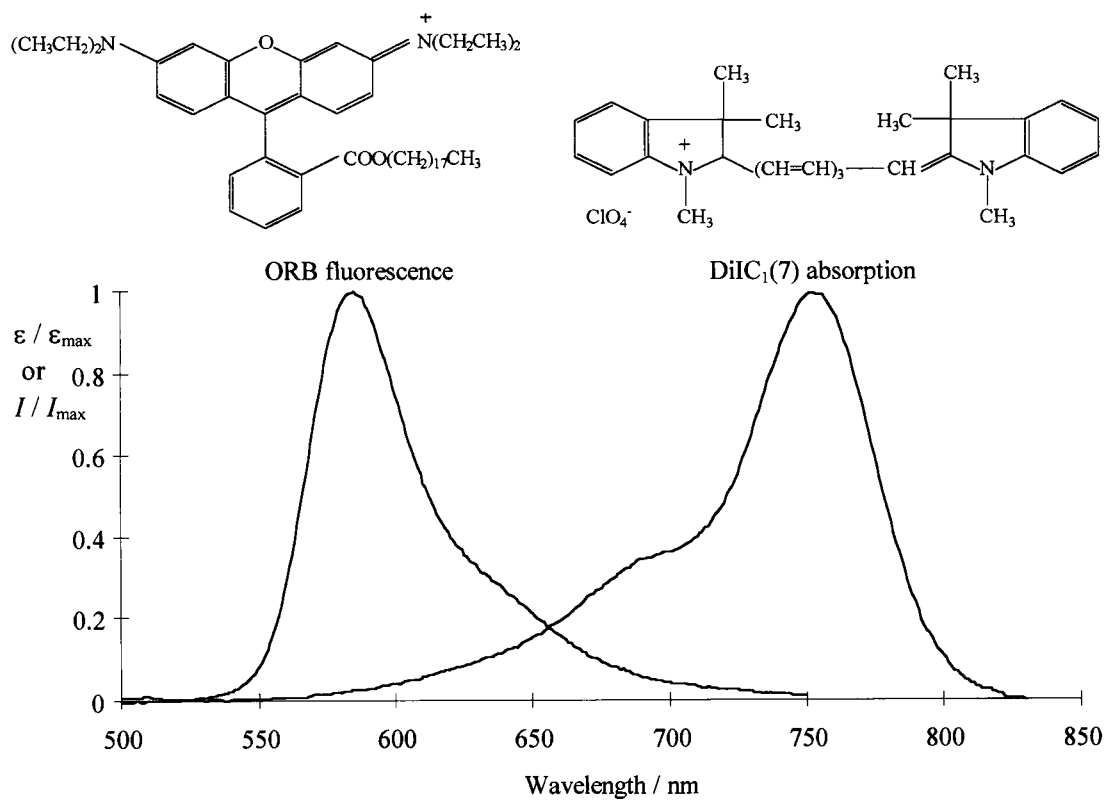

FIGURE 1 Structures of the ORB and $DiIC_1(7)$ probes and corrected normalized donor fluorescence (excitation at 475 nm) and acceptor absorption spectra.

Instrumentation

Fluorescence decay measurements were carried out with a time-correlated single-photon counting system. For excitation at 300 nm, a frequency doubled, cavity dumped (3.7 MHz repetition rate), dye laser of Rhodamine 6G (Coherent 701–2), synchronously pumped by a mode-locked Ar^+ laser (514.5 nm, Coherent Innova 400–10) was used. Two cutoff filters (Corion LG-400 and LS-650) were added to a Jobin-Yvon HR320 monochromator, to further screen scattered excitation light and isolate donor fluorescence from that of acceptor. For the detection, an Hamamatsu R-2809 MCP photomultiplier was used, and the instrumental response functions (80 ps fwhm) for deconvolution were generated from a scatter dispersion (silica, colloidal water suspension, Aldrich, Milwaukee, WI). Emission (at 585 nm) was detected at the magic angle relative to the vertically polarized excitation beam. The number of counts on the peak channel was 20,000, and the number of channels per curve used for analysis was 300, with time scales 20.4 ps per channel for the gel phase experiment, and 11.3 ps per channel for the fluid phase experiment. Data analysis was carried out using a nonlinear, least squares iterative convolution method based on the Marquardt algorithm (Marquardt, 1963). The goodness of the fit was judged from the χ^2_G, and weighted residuals and autocorrelation plots.

Fluorescence steady-state measurements were carried out with a SPEX F112 A Fluorolog spectrofluorometer, in a right-angle geometry. Excitation light was vertically polarized and fluorescence was detected at the magic angle. Correction of excitation and emission spectra was performed using a Rhodamine B quantum counter solution and a standard lamp, respectively (Lakowicz, 1983). Quartz cuvettes (5 mm × 5 mm) were used, and in these experimental conditions, no correction for artifacts was needed (Coutinho and Prieto, 1993). Temperature was controlled to ±0.5°C by a thermostatted cuvette holder. Fluorescence intensities were measured at 560 nm excitation and 585 nm emission wavelengths, respectively, with both emission and excitation spectral bandwidths of 9.0 nm. Absorption spectra were carried out in a Jasco V-560 spectrophotometer.

For evaluation of the critical radius of energy transfer, R_0, a rewritten Förster's formula (Berberan-Santos and Prieto, 1987) was used:

$$R_0 = 0.2108 \cdot \left[\kappa^2 \cdot \Phi_D \cdot n^{-4} \cdot \int_0^\infty I(\lambda) \cdot \epsilon(\lambda) \cdot \lambda^4 \cdot d\lambda\right]^{1/6} \quad (20)$$

where R_0 is expressed in angstroms, κ^2 is the orientation factor, Φ_D is the donor quantum yield in the absence of acceptor, n is the refractive index of the medium, $I(\lambda)$ is the normalized donor emission spectrum, and $\epsilon(\lambda)$ is the acceptor molar absorption coefficient in $M^{-1} \cdot cm^{-1}$ units. Wavelength is expressed in nm units. For the orientation factor, the value $\kappa^2 = 2/3$ (corresponding to a dynamic isotropic regime) was assumed (see Discussion), and $n = 1.33$ (water) was considered, attending to the solvatochromic behavior of ORB (Johansson and Niemi, 1987). ORB quantum yield in DPPC vesicles was approximated to the value in dioleylphosphatidylcholine ($\Phi = 0.55$ at 25°C; Johansson and Niemi, 1987). Based on this value, we determined $\Phi = 0.29$ at 50°C for the DPPC vesicles. The probes' absorption was observed to be smaller in vesicles than in ethanol. ϵ_{max} ($DiIC_1(7)$, 751 nm) = 156×10^3 $M^{-1} \cdot cm^{-1}$ was determined and used in Eq. 21 for calculation of R_0(ORB/$DiIC_1(7)$). For ORB, ϵ_{max}(25°C) = 67×10^3 $M^{-1} \cdot cm^{-1}$ and ϵ_{max}(50°C) = 58×10^3 $M^{-1} \cdot cm^{-1}$ were determined and used in Eq. 21, for calculation of R_0(ORB/ORB).

The steady-state anisotropy, $\langle r \rangle$, was calculated from (Lakowicz, 1983)

$$\langle r \rangle = (I_{VV} - G \cdot I_{VH})/(I_{VV} + 2 \cdot G \cdot I_{VH}) \quad (21)$$

where the different intensities are the steady-state vertical and horizontal components of the fluorescence emission with excitation vertical (I_{VV} and I_{VH}, respectively) and horizontal (I_{HV} and I_{HH}, respectively) to the emission axis. The latter pair of components is used to calculate the G factor ($G = I_{HV}/I_{HH}$).

For surface concentration determination, values of 52.3 and 72.1 $Å^2$ were assumed for the DPPC polar head areas in the $L_{\beta'}$ and L_α phases, respectively (Marsh, 1990), and only half of the lipid molecules (outer monolayer) were considered for this purpose (see Discussion).

RESULTS

Probe photophysics

Fig. 1 shows the donor (ORB) emission spectra, as well as the acceptor ($DiIC_1(7)$) absorption in the presence of a suspension of DPPC vesicles. A significant red shift is observed when the spectral maxima values ($\lambda_{max,abs}$(ORB) = 560 nm, result not shown; $\lambda_{max,em}$(ORB) = 585 nm, $\lambda_{max,abs}$($DiIC_1(7)$) = 752 nm) are compared to those in ethanol ($\lambda_{max,abs}$(ORB) = 555 nm and $\lambda_{max,em}$(ORB) = 577 nm (Johansson and Niemi, 1987), $\lambda_{max,abs}$($DiIC_1(7)$) = 741 nm (Brackmann, 1986)).

A monoexponential decay was observed for ORB in methanol ($\tau = 1.99$ ns, $\chi^2 = 1.147$). However, when the probe is incorporated in the vesicles, it is only possible to adequately describe it by allowing an additional (smaller and faster) component. For the sample with no acceptor, we recovered from single-curve analysis (using Eq. 3) $\tau_1 = 0.66$ ns ($A_1 = 0.24$), $\tau_2 = 2.89$ ns ($A_2 = 0.76$) at 25°C and $\tau_1 = 0.54$ ns ($A_1 = 0.18$), $\tau_2 = 1.51$ ns ($A_2 = 0.82$) at 50°C. This was not concomitant with any dependence of the emission spectrum on the excitation wavelength.

It should be stressed that, at the low probe to lipid ratios used, no spectral alteration of the acceptor absorption was observed, and the donor absorption is also characteristic of its monomeric form (Valdes-Aguilera and Neckers, 1989).

Steady-state ET

From the spectral data of Fig. 1 (spectra are lipid-phase insensitive), and the parameters described in Materials and Methods, Förster radii of $R_0 = 52.2$ Å (25°C, gel phase) and $R_0 = 46.8$ Å (50°C, liquid crystalline phase) were determined from Eq. 21.

In Fig. 2 the variation of the relative donor fluorescence intensities I_{DA}/I_D versus the acceptor concentration is depicted, both for probes incorporated in liquid crystalline and gel lipid systems. In both cases, a monotonic variation is obtained, the quenching being greater in the gel phase.

For the theoretical expectation of energy transfer in two dimensions, the Snyder and Freire (1982) approach was used. This requires the estimation of the distance of closest approach between donor and acceptor, L. For this purpose the method of atomic volume increments (Edward, 1970) was used, which led to the value $L = 9.4$ Å. In this way it is concluded that $R_0/L > 4$, i.e., there is no significant excluded volume effect, and the 2D curves represented in Fig. 2 are drawn from Eqs. 23 and 24 of the previously cited reference.

For the theoretical variation in 1D, see Fig. 2 *B*, Eq. 16 of this work was used. For this purpose the acceptor linear density was estimated from the time-resolved data (see

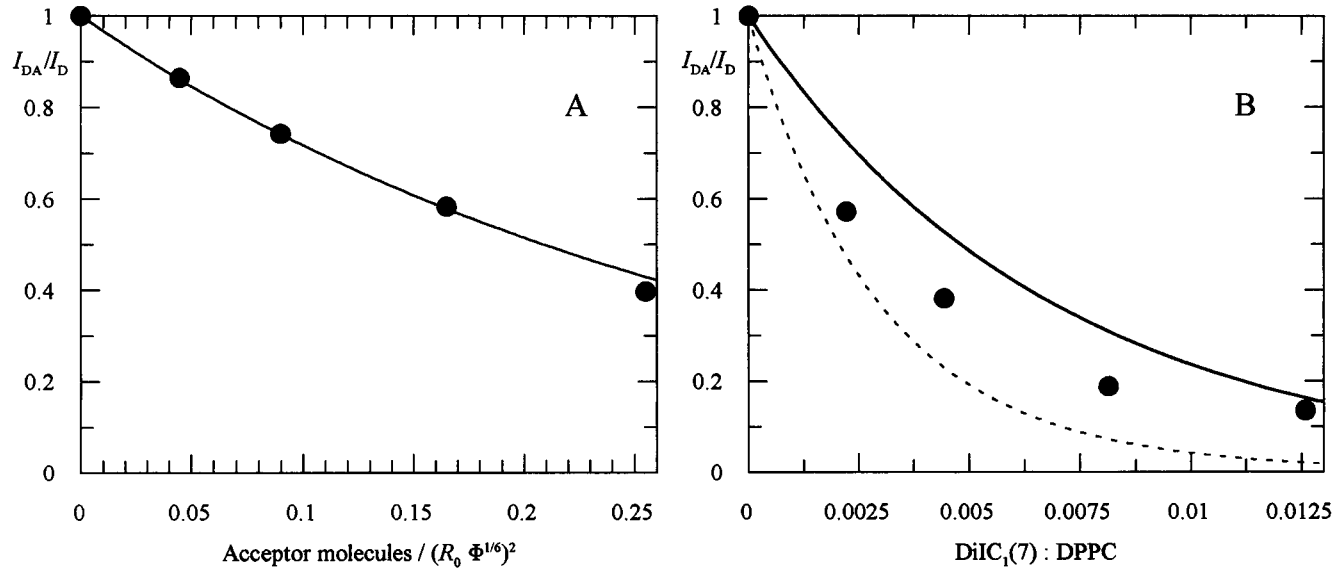

FIGURE 2 Steady-state relative fluorescence intensity I_{DA}/I_D versus acceptor concentration. (*A*) Fluid phase (50°C) results: experimental data (●) and theoretical 2D curve (Snyder and Freire, 1982) assuming R_0 = 46.8 Å (—). (*B*) Gel phase (25°C) results: experimental data (●), theoretical 2D curve (Snyder and Freire, 1982) assuming R_0 = 52.2 Å (*solid line*), and theoretical 1D curve (Eq. 18) additionally assuming l = 0.32 Å/DPPC molecule (*dotted line*; see text).

next). From inspection of Fig. 2 *A*, it can be concluded that the 2D ET theoretical prediction totally agrees with the experimental data for the liquid crystalline phase. On the contrary, no satisfactory fit is obtained in the gel phase, the apparent quenching was between those expected for 2D and 1D. The disagreement between the 2D curve and experimental data could be accounted for assuming static quenching. However, the fluorescence of $DiIC_1(7)$ is not quenched by ORB in membranes, ruling out such effect in this concentration range. In homogeneous medium (methanol solution), rhodamine B acted as a quencher of $DiIC_1(7)$ (results not shown).

A high steady-state anisotropy value of ORB in the lipid gel phase was obtained ($\langle r \rangle$ = 0.29 for ORB:DPPC = 1:1800) which is characteristic of a strongly immobilized probe. A smaller value was measured for the same probe in the liquid crystalline phase ($\langle r \rangle$ = 0.26 for the same ORB:DPPC ratio). The variation of ORB anisotropy was also studied as a function of the probe concentration, in the absence of $DiIC_1(7)$. In Fig. 3 the experimental data are

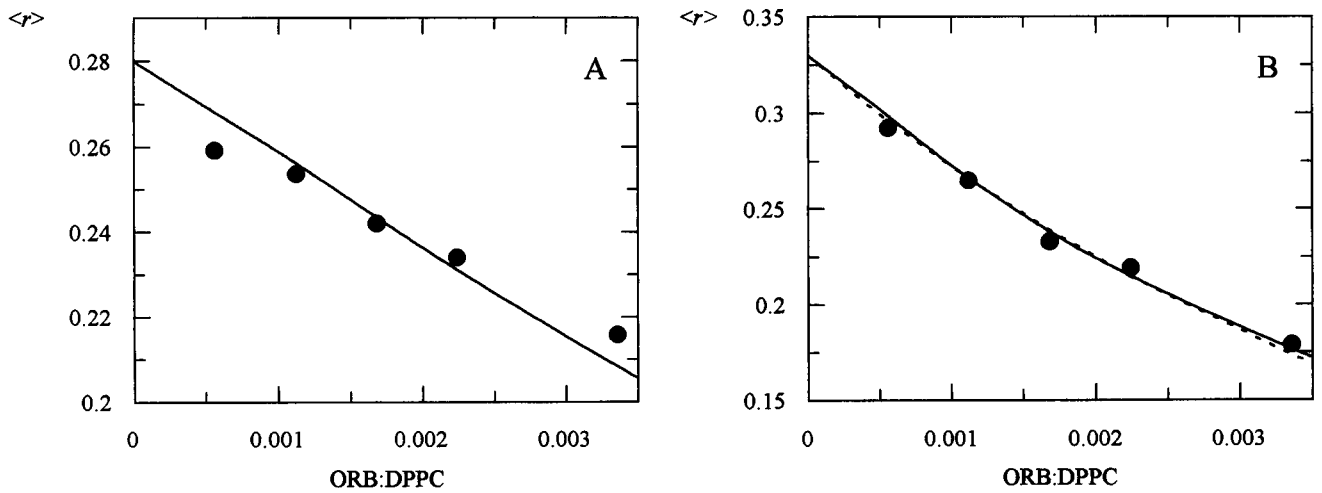

FIGURE 3 ORB steady-state fluorescence anisotropy $\langle r \rangle$ versus ORB:DPPC ratio. (*A*) Fluid phase (50°C) results: experimental data (●) and theoretical 2D curve (Snyder and Freire, 1982) assuming R_0 = 47.4 Å and $\langle r \rangle$ (infinite dilution) = 0.28 (—). (*B*) Gel phase (25°C) results: experimental data (●), theoretical 2D curve (Snyder and Freire, 1982) assuming R_0 = 54.2 Å, and $\langle r \rangle$ (infinite dilution) = 0.33 (*solid line*) and theoretical 1D curve (Sienicki et al., 1989) additionally assuming l = 0.32 Å/DPPC molecule (*dotted line*; see text).

compared to the 2D Snyder and Freire (1982) curve (Table 1 of their work). In these plots, we used R_0(ORB-ORB, 25°C) = 54.2 Å and R_0(ORB-ORB, 50°C) = 47.4 Å, calculated from Eq. 21. A reasonable agreement is obtained for the liquid crystalline phase (*A*). For the gel phase data (*B*), we also represented the two-particle model using the acceptor linear density estimated from the time-resolved data (see next). For this purpose, Eqs. 17–20 of this work were used, and the obtained anisotropies were normalized (i.e., divided by 0.4) and then multiplied by the extrapolated values at infinite dilution (0.33 at 25°C, 0.28 at 50°C). Both 1D (assuming this linear dimension value) and 2D transfer geometries agree well with the experimental points.

Time-resolved ET

Fig. 4 shows the fluorescence decays for DPPC LUV (50°C, liquid crystalline phase) incorporated with a fixed amount of ORB (ORB:DPPC = 1:10,000) and increasing concentrations of $DiIC_1(7)$. These data were globally analyzed according to Eq. 10, with fixed dimensionality $d = 2$ (Table 1). If d is left as an optimizing parameter, $d = 2.12$ is recovered. The remaining parameters are only slightly altered by this procedure, as can be seen in Table 1. In any case, acceptable χ^2 values and residuals and autocorrelation plots are obtained.

In Fig. 5, χ^2_G is plotted as a function of each linking parameter. For each curve, one parameter at a time was fixed at a predetermined value (different predetermined values of the same parameter correspond to different abscissas within the same curve), and the resulting χ^2_G value was registered. The 1 SD confidence interval (probability level 67%) is also represented. The main result is that $d = 2$ lies within the dimensionality interval [1.97, 2.28].

Table 2 shows the fitting parameters for the gel phase decay experiments (25°C). If the dimensionality is allowed to fluctuate, a value $d = 0.83$ is recovered, but the χ^2_G value is considerably worse than for the liquid crystalline system. Such a low d value suggests that our system has lower dimensionality than the expected (and verified for the fluid phase decays) 2D. Fixing integer dimensionalities, the decay kinetics are in fact better described by the 1D model rather than by 2D ET (strong increase in the χ^2_G value).

A further model verification would be the linear variation of the C parameter versus acceptor concentration (Eq. 1). In addition, from Eq. 2, it is clear that this plot gives the Förster radius R_0 from the slope. In case of a complex decay, Eq. 10 holds, and two Förster radii, R_{01} and R_{02}, are obtained. In this way, an average value, $\langle R_0 \rangle$, should be determined and compared with the value determined from spectroscopic data, R_0. $\langle R_0 \rangle$ is derived as

$$\langle R_0 \rangle^d / \langle \tau \rangle^{d/6} = \langle R_{01} \rangle^d / \langle \tau_1 \rangle^{d/6} = \langle R_{02} \rangle^d / \langle \tau_2 \rangle^{d/6} \quad (22)$$

where $\langle \tau \rangle$ is the average lifetime,

$$\langle \tau \rangle = (A_1 \cdot \tau_1^2 + A_2 \cdot \tau_2^2)/(A_1 \cdot \tau_1 + A_2 \cdot \tau_2) \quad (23)$$

In Fig. 5 *A* the 2D c parameter (Eq. 10) for the fluid phase experiment is plotted versus n_{2A}. The experimental points are very closely described by a linear fit. From the slope one calculates $\langle R_0 \rangle = 48.1$ Å, in close agreement with the spectroscopic $R_0 = 46.8$ Å. The gel phase 2D c parameter representation gives $\langle R_0 \rangle = 52.0$ Å (result not shown), also in agreement with the spectroscopic value $R_0 = 52.2$ Å. However, the fitting quality is worse than in the liquid crystalline system.

For the 1D fit, it is not possible to compute a linear density of acceptor, n_{1A}, so we were not able to recover $\langle R_0 \rangle$. In this case, we did it the other way around. We used the spectroscopic R_0 to compute the linear density. In this way, introducing the known acceptor:lipid ratio, the average length per DPPC molecule (l) is calculated. We obtained $l = 0.32$ Å. This was the value used to plot the steady-state fluorescence intensity versus acceptor/lipid ratio in Fig. 2 *B*, and the 1D concentration depolarization curve in Fig. 3 *B*. As stated above, the heterotransfer plot disagreed with the experimental data (a good fit to these results would require $l = 0.46$ Å, result not shown), unlike the homotransfer curve, which describes the measured anisotropy.

We also analyzed both fluid phase and gel phase results according to Eq. 13, where a term for nontransferring donors is included. Although for the fluid phase data there is no improvement in the fitting statistics (results not shown), the gel phase results are statistically much better described by this model (see Table 3). Contrary to what we observed when analyzing using Eq. 10, we obtained a much better fit with $d = 2$, and if this parameter is not fixed beforehand, $d = 2.14$ is recovered (close to the value obtained for fluid phase using Eq. 10, and to the expected 2D value), with a small reduction in χ^2_G relative to the $d = 2$ case (once again, this case is within the uncertainty interval for d; result not shown). Moreover, although a nonmonotonic variation of r with c is observed when d is fixed at 1D (which has no physical significance), when $d = 2$ the recovered r decreases continuously with increasing c (as seen in Table 4).

We also plotted c versus n_{dA} using these fitting results. For the 1D fit, the recovered l value ($l = 0.29$ Å) shifts a little further away from the best steady-state value. For the 2D fit, we now recover $\langle R_0 \rangle = 63.9$ Å, in clear disagreement with the spectroscopic value.

DISCUSSION

Probe photophysics

The measured spectra of both probes are identical to reported data (Brackmann, 1986; Johansson and Niemi, 1987). The observed red shift is clear evidence for probe interaction with the vesicle. For the used lipid concentrations, the cyanine dye incorporates quantitatively in the lipidic phase, the same happening to the aliphatic-tail-derivatized rhodamine. In addition, because of their electric charge (see Fig. 1) both chromophores are adsorbed at the water-lipid interface, evidence for ORB

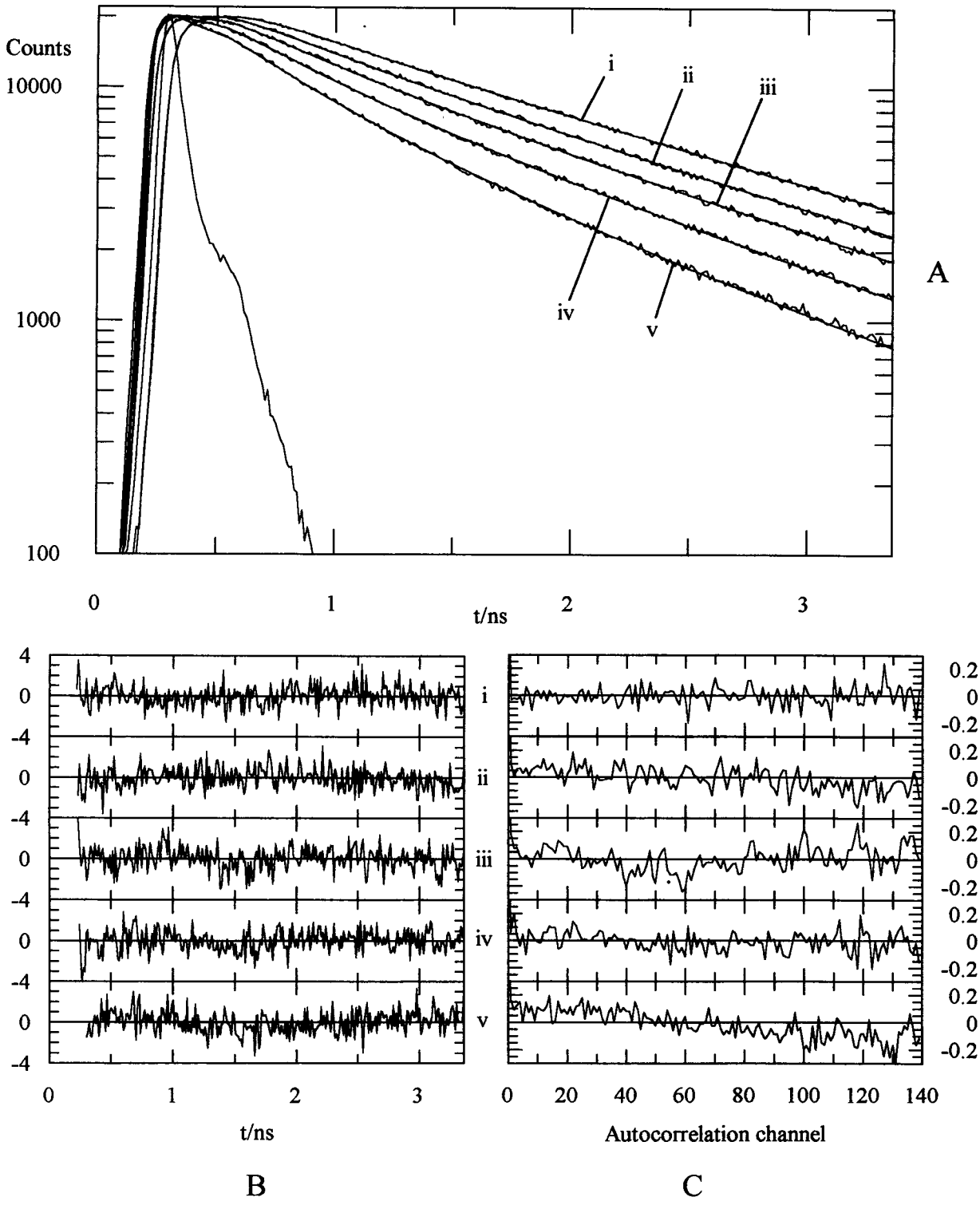

FIGURE 4 (*A*) Time-resolved fluorescence intensity of ORB in fluid phase (50°C) DPPC vesicles, for different $DiIC_1(7)$ concentrations ($DiIC_1(7)$ to DPPC ratio: i) 0; ii) 1:900; iii) 1:450; iv) 1:245; v) 1:160). The laser pulse profile is represented, and the smooth lines are best fit curves (global analysis) of Eq. 10 ($d = 2$; see Table 1). (*B*) Weighted residuals plots. (*C*) Autocorrelation function plots.

being reported by Johansson and Niemi (1987). In this way, no internalization should be considered for the purpose of energy transfer kinetics, as derived by Davenport et al. (1985).

At the low ORB to lipid ratio used (ORB:DPPC = 1:10000), there is no energy migration between the rhodamine chromophores, as concluded from the anisotropy study of Johansson (Johansson and Niemi, 1987) and our

TABLE 1 Best fit parameters of Eq. 10, for the global analysis of the fluorescence decay of ORB incorporated in DPPC LUV (50°C, fluid phase), in the presence of $DiIC_1(7)$

	τ_1/ns	τ_2/ns	A_1/A_2	d	χ^2_G
Variable dimensionality	0.67	1.57	0.32	2.12	1.213
Fixed dimensionality (2D)	0.73	1.59	0.37	2 (Fixed)	1.223

data. This is crucial for our study, because the occurrence of migration between donors would bias the heterotransfer data. From the absorption spectrum of $DiIC_1(7)$, there is no evidence of aggregate (dimer) formation. This is a further simplification, because in this situation there is no need to consider two acceptor species (Faria et al., 1989).

The ORB fluorescence decay in vesicles, as previously referred, is biexponential. The larger components in gel phase (τ = 2.89 ns) and liquid crystalline phase (τ = 1.51 ns) compare with published values for similar probes with the same chromophore (Medhage et al., 1992; Ballet et al., 1996). In addition, a smaller and faster component (500–700 ps) was also detected.

It is not unusual that complex decays are observed for fluorescent probes in interaction with microheterogeneous systems. Recent examples are the decays of an indole derivative bound to DNA (Maliwal et al., 1995) and an NBD derivative in vesicles (Duportail et al., 1995). Specifically for the rhodamine chromophore incorporated in Langmuir-Blodgett multilayer films, a similar complex decay was observed, with a smaller (22%) and faster (1.40 ns) component (Ballet et al., 1996). As in our work, these authors also observed a monoexponential decay in homogeneous medium, ruling out the presence of a significant impurity emission. The simultaneous emission of both protonated and unprotonated xanthene moieties of rhodamine was also discarded in their work (in our study an ester derivative was used, totally precluding this source of complex decay), as well as a

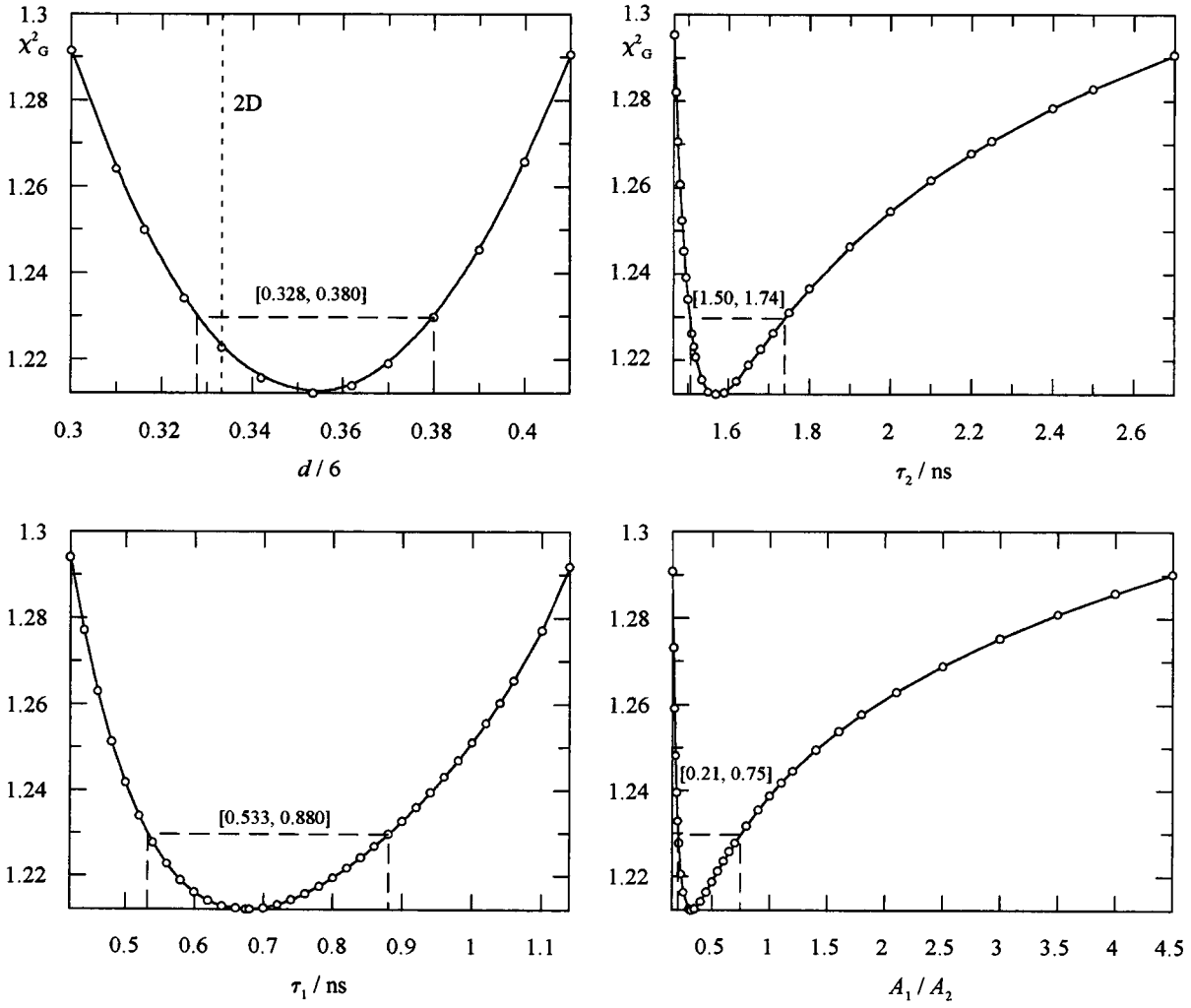

FIGURE 5 χ^2_G as a function of each linking parameter, for the analysis of the fluid phase (50°C) time-resolved data of ORB fluorescence, using Eq. 10. Also shown are the confidence intervals for these parameters, at a significance level of 67% (note that the expected 2D value, $d/6$ = 0.333, lies within the respective interval).

TABLE 2 Best fit parameters of Eq. 10, for the global analysis of the fluorescence decay of ORB incorporated in DPPC LUV (25°C, gel phase), in the presence of $DiIC_1(7)$

	τ_1/ns	τ_2/ns	A_1/A_2	d	χ^2_G
Variable dimensionality	0.79	2.99	0.38	0.83	1.909
Fixed dimensionality (2D)	0.50	2.95	0.42	2 (Fixed)	4.939
Fixed dimensionality (1D)	0.73	2.97	0.37	1 (Fixed)	1.980

TABLE 3 Best fit parameters of Eq. 13, for the global analysis of the fluorescence decay of ORB incorporated in DPPC LUV (25°C, gel phase) in the presence of $DiIC_1(7)$

	τ_1/ns	τ_2/ns	A_1/A_2	d	χ^2_G
Variable dimensionality	0.68	2.90	0.31	2.14	1.088
Fixed dimensionality (2D)	0.70	2.91	0.32	2 (Fixed)	1.095
Fixed dimensionality (1D)	0.79	2.99	0.38	1 (Fixed)	1.544

continuous population of conformers due to different rotational angles of the benzoic acid/benzoate group and the xanthene.

Although the origin of the faster component (probably associated with probes in distinct adsorbed configurations) is not clear, this does not hamper the ET study. In fact, 1) from the polar nature of the chromophore, the two emissive species are expected to be located at the lipid-water interface, and certainly not deeply incorporated inside the bilayer, and 2) from the emission invariance with excitation wavelength, it can be concluded that the main differences between the two species are essentially their nonradiative pathways, both having identical radiative rate constants k_F. This validates the application of Eqs. 10 and 13 for the donor decay in the energy transfer study.

We are aware that the complex decay could eventually be described by a distribution of lifetimes (James et al., 1985), and this can be easily considered in the Förster-type kinetics. This approach was not taken because the two discrete components used are totally satisfactory from the standpoint of statistical criteria. In addition, this would introduce a formalism that is too cumbersome and the data analysis would possibly be model insensitive.

Steady-state ET

Although the most rigorous study of model fitting is obtained from time-resolved data, the steady-state fluorescence ET measurements allow a first quantitative evaluation of the system dimensionality and/or distance distribution function of acceptors. In addition, by comparison with the time-resolved data, it can elucidate the eventual contribution of static quenching mechanisms.

As shown in Fig. 2 *A*, the theoretical prediction assuming random distribution of probes in 2D is in total agreement with the experimental data for the liquid crystalline phase. This further validates 1) the assumption made for determining the acceptor density; due to the long flip-flop time of the probes, energy transfer can be considered to be restricted to the outer membrane leaflet, i.e., there is no probe translocation; and 2) the utilization of the theoretical curves, which were derived for a monoexponential donor (Snyder and Freire, 1982). The integrated time dependence of a complex decay (each component characterized by a different lifetime and a different Förster radius) can be reasonably described by the integration of a single (mean) lifetime decay, taking into account the spectroscopic R_0.

For the gel phase system, no agreement was obtained with a 2D random distribution. ET is more efficient than expected, although still less than predicted for 1D transfer geometry, using the time-resolved l value (0.32 Å/DPPC molecule). To establish whether static quenching could be taking place, we measured the $DiIC_1(7)$ fluorescence in the presence and absence of ORB (probe concentration values were equal to those used in the ET experiment). No quenching was observed. However, in methanol solution $DiIC_1(7)$ fluorescence is indeed quenched when the rhodamine B concentration was increased (results not shown). We can therefore safely conclude that no dark ground-state ORB-$DiIC_1(7)$ complexes are being formed in our ET experiment, and the observed deviation is not due to static quenching. Therefore, our results point to a restriction of the system dimensionality, or to a distribution function in which donor and/or acceptor aggregation are assumed.

We tried to obtain independent information on the donor distribution function by carrying out a study of energy migration among ORB molecules (Fig. 3). The results suggest that this probe may be randomly distributed even in the gel phase (although it could still be randomly distributed in a 1D geometry, for the 1D depolarization curve fits the results equally well), and consequently the failure of the 2D steady-state heterotransfer analysis (or 1D, for that matter) for this phase indicates the nonrandomness of acceptor distribution. It would be interesting to perform a similar study for the $DiIC_1(7)$ molecule. However, its fluorescence is rather weak, thus precluding good quality polarization measurements.

Detailed studies of ET in gel phase are, to our knowledge, very scarce in the literature, particularly on the striking

TABLE 4 Variation of the recovered r parameter using Eq. 13 for analysis of the fluorescence decay of ORB incorporated in DPPC LUV (25°C, gel phase) in the presence of $DiIC_1(7)$, assuming both $d = 1$ and $d = 2$ values

$DiIC_1(7)$:DPPC	0.0022	0.0044	0.0082	0.0126
r(2D fit)	0.67	0.35	0.04	0.02
r(1D fit)	1.3×10^{-6}	7.1×10^{-3}	4.3×10^{-4}	1.8×10^{-3}

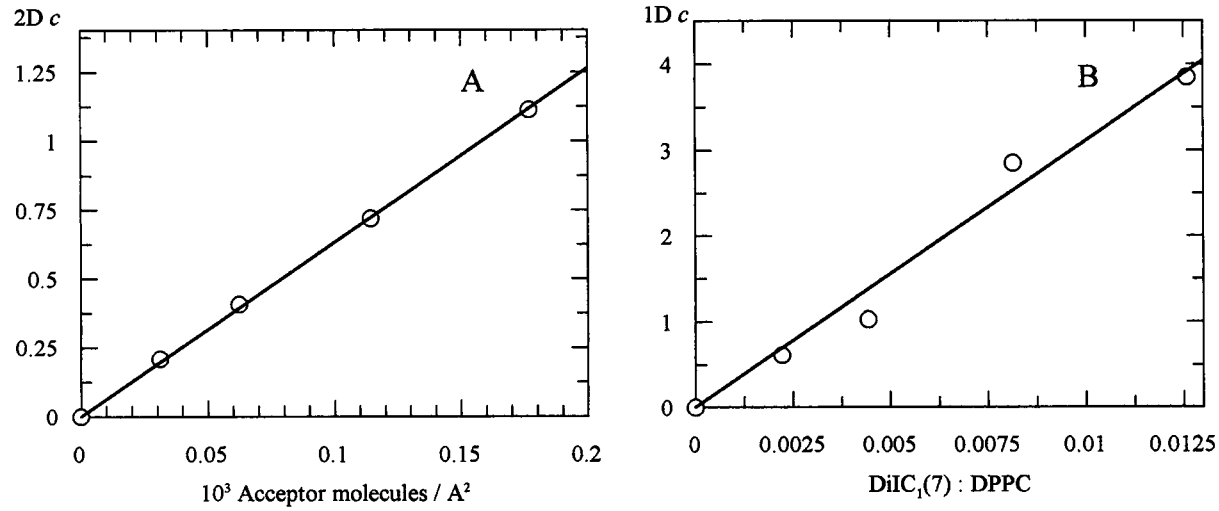

FIGURE 6 (*A*) 2D c parameter recovered from fitting the fluid phase (50°C) time-resolved data to Eq. 10 with $d = 2$, as a function of acceptor surface density (○). From the slope of the linear fit (—), $\langle R_0 \rangle = 48.1$ Å is obtained (compare with the spectroscopic value, $R_0 = 46.8$ Å). (*B*) 1D c parameter recovered from fitting the gel phase (25°C) time-resolved data to Eq. 10 with $d = 1$, as a function of acceptor to lipid ratio (○). From the slope of the linear fit (—), and using the spectroscopic R_0 value (52.2 Å), $l = 0.32$ Å/DPPC molecule is obtained (see text).

difference from the fluid phase for the same donor-acceptor pair. As shown below, the works by Tamai et al. (1987) and Duportail et al. (1995) are rather controversial.

Time-resolved ET

The fluid phase results show excellent agreement with theory, considering a 2D random distribution of acceptors. This may seem like a trivial conclusion because the geometrical approximation from a spherical vesicle to a planar sheet is verified. The curvature effect is negligible when the sphere diameter D and the Förster radius R_0 obey the relationship $D/R_0 > 1.5$ (Eisinger et al., 1981), which is clearly the case. However, to our knowledge, this is the first experimental verification of such kinetics from time-resolved experiments in vesicles. The decay law considering $d = 2$ satisfies the experimental data, and additionally $d = 2.00$ lies within the 1 SD confidence interval (Fig. 5). In this way there is no need to invoke a noninteger dimensionality, i.e., a fractal geometry or a model with isolated donors because analysis using Eq. 13 does not give a better fit.

Recently a fractal formalism was used to rationalize the ET interaction between NBD-labeled phosphatidylethanolamine (donor) and *N*-(lissamine-rhodamine B)-labeled phosphatidylethanolamine (acceptor) in lipid vesicles (Duportail et al., 1995). This is certainly due to the ability of a two-term stretched exponential (Eq. 1 in the above cited reference) to describe any complex fluorescence decay. However, these authors invoke a diffusion controlled type of interaction, which is totally incorrect, because the Förster radius for this pair is quite significant ($R_0 \sim 40$ Å for a NBD-family/Rhodamine-family ET pair, Van der Meer et al., 1994), i.e., no diffusion is operative in the quenching process in a model system of membranes.

The gel results are strikingly different from those of the liquid crystal. As shown in Table 2, a very high χ^2_G value is obtained when analyzing the decay with Eq. 10 and $d = 2$. When the dimensionality is allowed to float, a value $d = 0.83$ is recovered, and the goodness of fit is very close to that obtained with exact dimensionality $d = 1$. These results suggest a reduction of the apparent system dimensionality.

A detailed gel-phase time-resolved study was carried out by Tamai et al. (1987), using rhodamine 6G (donor) and malachite green (acceptor). Their data could not be well described by a random 2D Förster-type equation, and a satisfactory agreement was obtained using a superposition of 2D and 3D kinetics. There is no physical basis for this analysis because these polar dyes do not penetrate inside the vesicles. The 3D contribution is merely taking into account a nonuniform distribution of probes, in which the molecules are at closer distance than expected on the basis of a random distribution. In any case, these authors' results point to an overall increase in dimensionality, at variance with ours.

The eventual implications of the orientation factor κ^2 (Eq. 21) in our study should be discussed. As stated above, from the fitting of Eqs. 10 and 13 to the data, the c parameter is recovered. It is related to the product of the acceptor density times R_0^d (Eq. 2), so a $\langle R_0 \rangle$ value can be calculated from the time-resolved experiment (Eqs. 23–24), independently of the κ^2 value assumed for the calculation of the spectroscopic R_0 (Eq. 21). A comparison between $\langle R_0 \rangle$ and R_0 should be made, and certainly the deviation between these values should be discussed on the basis of the orientation factor, e.g., as done by Maliwal et al. (1995). This is the only way in which the implications of the κ^2 value are to be taken into consideration regarding the time-resolved experiment. Because the actual spectroscopic R_0 value is never used in the decay-data analysis, all recovered parameters,

including the dimensionality, are free from κ^2 uncertainties. In any case, whether the system is better described by the static or the dynamic limit, and independently of the donor/acceptor dipole angular distribution, the decay law will still be described by the presented formalism, apart from the actual changes in κ^2, which, as stated above, do not affect the recovered parameters. This expression may not be valid if the system had a finite size on a molecular scale or there were considerable excluded volume effects (Baumann and Fayer, 1986), which is avoided by choosing convenient experimental conditions (large lipid vesicles and moderate probe concentrations), or if the donor or acceptor distributions were no longer random.

The relevance of orientation effects on electronic ET has received careful attention in the literature (for a recent review see Van der Meer et al., 1994). In our work, the dynamically averaged isotropic value, $\kappa^2 = 2/3$, was considered for calculation of the R_0 value used for the theoretical curves in the steady-state plots (Figs. 2 and 3). We are aware that this situation is not verified, i.e., the system is not isotropic and not strictly dynamic, as concluded from the high ORB anisotropy values ($\langle r \rangle = 0.29$ for gel; $\langle r \rangle = 0.26$ for liquid crystal; ORB:DPPC = 1800). Still in the dynamic regime, a more accurate description would be to consider a 2D system, with donor dipole orientation allowed in a hemisphere and acceptor dipole oriented along the surface plane. For this geometry, which seems to be closer to one of our Förster pair (donor = derivatized rhodamine, acceptor = cyanine), the κ^2 value is 5/6 (Eisinger et al., 1981), very close to $\kappa^2 = 2/3$. As can be seen from Eq. 21, the R_0 dependence on $(\kappa^2)^{1/6}$ strongly mitigates all noncritical uncertainties (e.g., the use of $\kappa^2 = 5/6$ instead of 2/3 changes R_0 by <4%). This is corroborated by the agreement between the spectroscopic values, $R_0 = 52.2$ Å (gel phase) and $R_0 = 46.8$ Å (liquid crystalline phase), and the model-derived ones, $\langle R_0 \rangle = 52.0$ Å and 48.1 Å, respectively. In ET experiments in microheterogeneous media, there is always uncertainty regarding the best values for both κ^2 and the refractive index n. We interpret the agreement between R_0 and $\langle R_0 \rangle$ in our work as indicating an appropriate choice of the parameter $a = (\kappa^2/n^4)^{1/6}$, which is proportional to R_0. Note that our choice ($\kappa^2 = 2/3$, $n = 1.33$) leads to $a = 0.773$. In a recent work (Mehage et al., 1992), a very similar system is studied (the fluorophore was Liss-RhB-PE rather than ORB), and from their linear dichroism studies, they conclude that the order parameter $S \approx -0.4$, almost the same as the ORB from a previous report, -0.36 (Johansson and Niemi, 1987). This should lead to transition dipoles almost parallel to the lipid bilayer, and to $\kappa^2 = 1.07$. For R_0 calculation these authors used $n = 1.45$. Combining these two values, they successfully used $a = 0.789$, which differs from our value in 2.1%. This combination would change our R_0 values in ~1 Å, which is less than the error associated with R_0 estimates. We therefore believe that even if the dipole distribution is not strictly isotropic, our R_0 value is correctly calculated.

Returning to the gel phase analysis, it is generally acknowledged that defect lines corrugate the lipid gel surface. In this situation, a very likely explanation for the bad 2D fit is to assume that the acceptor molecules segregate along the fluid-like gel domain boundaries. $DiIC_n$ probes' selectivity for lipid bilayer phases (for $10 \leq n \leq 22$) was studied by measuring shifts in the thermal transition temperature (Klausner and Wolf, 1980) and gel/fluid partition coefficients were determined by fluorescence quenching measurements (Spink et al., 1990). It was concluded that dyes with acyl chain length n less than that of DPPC (n = 16) prefer the fluid phase, and aggregate when forced to be in the gel. If we can extrapolate these results (obtained for a very similar system) to our study, for which $n = 1$, very strong aggregation of acceptor in the gel phase would be expected.

Assuming the existence of segregation to lipid domain boundaries, several factors would probably preclude the clean recovery of 1D ET dimensionality. 1) Segregation would never be complete, and there would still be a considerable amount of both probes dispersed in the gel domains (depending on the actual lipid phase selectivities); 2) the grain boundaries, far from being ideal lines, have finite (albeit small) width; and 3) in the confluence zone of three or more domains, there would be ET along multiple directions. If the domain size is small, many probe molecules would fall under this situation. Taking $l = 0.32$ Å/DPPC molecule, the ratio average length/area for DPPC LUV gel phase would be *l*/area of DPPC polar head = 0.32 Å/52.3 $Å^2 = 0.0061$ $Å^{-1}$. We can calculate the corresponding domain size assuming simple domain geometries. For a regular square grid, we would have ca. 2000 lipid molecules per domain, and for a hexagonal lattice, ca. 1750. In fact, these values agree with those of Sankaram et al. (1992) determined by electron spin resonance in a dimiristoylphosphatidylcholine/distearoylphosphatidylcholine mixture. These domains would indeed be very small (~300 Å), therefore deviations to 1D transfer kinetics due to this effect would probably be considerable. In this situation, the fact that a relatively high χ^2_G value is obtained would not per se exclude the validity of 1D ET kinetics. That was the reason that led us to the ORB anisotropy study. However, as pointed out above, this experiment did not clarify the question.

A random acceptor aggregation (i.e., one not invoking domain boundaries) could in principle also be contemplated. In this case, a 2D formalism would hold, provided that a smaller effective surface density (not completely balanced by the slight increase in R_0) was used. Altogether, this would imply that the steady-state experimental points in Fig. 2 *B* (full circles) would then shift to the left, with a great deviation from the universal 2D curve (full line). Additionally, no spectral evidence of $DiIC_1(7)$ dimers was observed; in this way, this situation seems very unlikely.

The eventual existence of donors distant from the defect lines and therefore relatively isolated from acceptors inspired us to analyze our data using Eq. 13, as previously done by others (Yamazaki et al., 1987; Ohta et al., 1993; Ballet et al., 1996). As can be seen in Table 3, there is a

remarkable improvement in χ^2_G, most impressively when $d = 2$ is assumed. Moreover, for this d value, the r parameter decreases with increasing c (see Table 4), as expected, because as c increases, fewer donors would be isolated (Yamazaki et al., 1987; Ohta et al., 1993). Of course, with increasing c, the ratio of acceptors to donors becomes very large (>50 for the most concentrated sample) and thus there should always be acceptors in the vicinity of virtually every donor, even if segregation of $DiIC_1(7)$ is taking place (hence the decreasing r). However, 1) the r values for the lower acceptor concentrations seem exaggeratedly large (for the lowest concentration, ca. 40% of donors would be isolated) and 2) the recovered $\langle R_0 \rangle$ value (63.9 Å) is much higher than the spectroscopic value. We therefore believe that the good statistics of the fits are due to the fitting versatility of Eq. 13, rather than to actual isolation of donors. We would like to stress that a good fit by Eq. 13 does not necessarily mean that a fraction of donors would actually be totally isolated. It is probable that if the acceptor distribution is no longer random, e.g., due to segregation along domain boundaries, so that some donors (those furthest from the boundaries) would be more distant from the acceptor molecules, fitting with Eq. 13 would introduce a major statistical improvement relative to Eq. 10.

We integrated (Eq. 14) the gel phase fits assuming both Eqs. 10 (1D and 2D ET) and 13 (2D) to compare with the steady-state data (results not shown). By integration of the 1D and 2D fits, quenching ratios close to the respective theoretical curves are obtained (as expected, because the 1D curve assumes $l = 0.32$ Å from the 1D fit of the time-resolved data, and the 2D curve assumes $R_0 = 52.2$ Å, close to the value recovered from the 2D fit of the time-resolved data, $\langle R_0 \rangle = 52.0$ Å). These are not good statistical fits of the time resolved results, therefore it is not surprising that on integration one does not recover the steady-state-measured quenching. Integration of a better statistical fit (even if not physically significant) should fall closer to the steady-state values. We verified this using Eq. 13 and 2D ET. The integrated results are between the 1D and 2D curves and closer to the experimental steady-state values. This further excludes the existence of static quenching, and stresses the fact that ET in the gel phase cannot be adequately described admitting either 1D and 2D formalisms, which should not be due to some kind of fractal geometry, but to partial segregation of probes along grain boundaries.

CONCLUSIONS

A detailed energy transfer study, both in steady and transient state, between ORB (donor) and $DiIC_1(7)$ (acceptor) was carried out in a model system of membranes (DPPC LUV) in the gel and liquid crystalline phases.

The decay law for energy transfer in 2D, assuming random distribution of probes, was verified in the fluid phase using global analysis of decay data, ruling out a fractal geometry for this system. In agreement, no spectral evidence for formation of dimers of either probe was observed, and the steady-state energy transfer efficiency was correctly predicted.

At variance, the steady-state efficiency of energy transfer in the gel phase is between the values expected for 2D and 1D. Additionally, the decay data are better described by the 1D law. The eventual contribution of a static quenching mechanism was discarded, because no acceptor quenching by the donor was verified in membranes in this concentration range, unlike in homogeneous medium. A model assuming a population of nontransferring donors was also ruled out, due to the unrealistic recovered parameters, namely R_0. A study of donor energy migration was also carried out to obtain further information on the distribution function of this probe, but in this case the experiment was not conclusive regarding the verification of 1D or 2D dimensionality. The gel phase data indicate a reduction of the system dimensionality which was explained on the basis of the defect lines that corrugate the lipid gel surface. The probes, namely, the acceptor, are supposed to segregate along the fluid-like gel domain boundaries. Using the probe linear concentrations recovered from the time-resolved experiment, and assuming simple domain geometries, estimation of their size indicates small values (~1750-2000 molecules). Once again, the existence of a fractal dimension is ruled out.

This work was supported by Junta Nacional de Investigação Científica e Tecnológica (Portugal), programs PUEM/S/ERC/53/93, Ciência Subprograma III, Medida M and PECS/C/SAU/144/95. L.M.S.L. acknowledges a grant (BD 3927/94) from PRAXIS XXI (Portugal). A.F. acknowledges a grant from INVOTAN (Programa de cooperação "OUTREACH").

We acknowledge Dr. Mark Van der Auweraer for providing us with a copy of a submitted manuscript.

REFERENCES

Almeida, P. F. F., W. C. C. Vaz, and T. E. Thompson. 1992. Lateral diffusion and percolation in two-phase, two-component lipid bilayers: topology of the solid-phase domains in-plane and across the lipid bilayer. *Biochemistry.* 31:7198–7210.

Ballet, P., M. Van der Auweraer, F. C. De Schryver, H. Lemmetyinen, and E. Vuorimaa. 1996. Global analysis of the fluorescence decays of N, N′-dioctadecyl rhodamine B in Langmuir-Blodgett films of diacyl phosphatidic acids. *J. Phys. Chem.* In press.

Baumann, J., and M. D. Fayer. 1986. Excitation energy in disordered two-dimensional and anisotropic three-dimensional systems: effects of spatial geometry on time-resolved observables. *J. Chem. Phys.* 85: 4087–4107.

Beechem, J. M., E. Gratton, M. Ameloot, J. R. Knutson, and L. Brand. 1991. The global analysis of fluorescence intensity and anisotropy decay data: second-generation theory and programs. *In* Topics in Fluorescence Spectroscopy, Vol. 2: Principles. J. R. Lakowicz, editor. Plenum Press, New York. 241–305.

Berberan-Santos, M. N., and M. J. E. Prieto. 1987. Energy transfer in spherical geometry. Application to micelles. *J. Chem. Soc. Faraday Trans. 2.* 83:1391–1409.

Blumen, A., J. Klafter, and G. Zumofen, 1986. Influence of restricted geometries on the direct energy transfer. *J. Chem. Phys.* 84:1397–1401.

Brackmann, U. 1986. Lambdachrome® Laser Dyes. Lambda Physik GmbH, Göttingen, Germany.

Coutinho, A., and M. Prieto. 1993. Ribonuclease T_1 and alcohol dehydrogenase fluorescence quenching by acrylamide. *J. Chem. Ed.* 70: 425–428.

Davenport, L., R. E. Dale, R. H. Bisby, and R. B. Cundall. 1985. Transverse location of the fluorescent probe 1,6-diphenyl-1,3,5-hexatriene in model lipid bilayer membrane systems by resonance energy transfer. *Biochemistry.* 24:4097–4108.

Duportail, G., F. Merola, and P. Lianos. 1995. Fluorescence energy transfer in lipid vesicles. A time-resolved analysis using stretched exponentials. *J. Photochem. Photobiol. A. Chem.* 89:135–140.

Derzko, Z., and K. Jacobson. 1980. Comparative lateral diffusion of fluorescent lipid analogues in phospholipid multibilayers. *Biochemistry.* 19:6050–6057.

Edward, J. T. 1970. Molecular volumes and the Stokes-Einstein equation. *J. Chem. Ed.* 47:261–270.

Eisinger, J., W. E. Blumberg, and R. E. Dale. 1981. Orientational effect in intra- and intermolecular long range excitation energy transfer. *Ann. N. Y. Acad. Sci.* 366:155–175.

Eisenfeld, J., and C. C. Ford. 1979. A systems theory approach to the analysis of multiexponential fluorescence decay. *Biophys. J.* 26:73–88.

Even, U., K. Rademann, J. Jortner, N. Manor, and R. Reisfeld. 1984. Electronic energy transfer on fractals. *Phys. Rev. Lett.* 52:2164–2167.

Faria, J. L., M. Berberan-Santos, and M. J. E. Prieto. 1989. A comment on the localization of cyanine dye binding to brush-border membranes by the fluorescence quenching of *n*-(9-anthroyloxy) fatty acid probes. *Biochim. Biophys. Acta.* 1026:133–134.

Farinha, J. P. S., J. M. G. Martinho, A. Yetka, and M. A. Winnik. 1995. Direct nonradiative energy transfer in polymer interphases: fluorescence decay functions from concentration profiles generated by Fickian diffusion. *Macromolecules.* 28:6084–6088.

Hauser, M., U. K. A. Klein, and U. Gösele. 1976. Extension of Förster's theory of long range energy transfer to donor-acceptor pairs in systems of molecular dimensions. *Z. Phys. Chem.* 101:255–266.

Heimburg, T., and R. L. Biltonen. 1996. A Monte Carlo simulation study of protein-induced heat capacity changes and lipid-induced protein clustering. *Biophys. J.* 70:84–96.

Hui, S. W., and H. Yu. 1993. Electron diffraction studies of molecular ordering and orientation in phospholipid monolayer domains. *Biophys. J.* 64:150–156.

James, D. R., Y. S. Liu, P. de Mayo, and W. R. Ware. 1985. Distributions of fluorescence lifetimes: consequences for the photophysics of molecules adsorbed on surfaces. *Chem. Phys. Lett.* 120:460–465.

Johansson, L. B. A., and A. Niemi. 1987. Electronic energy transfer in anisotropic systems. 1. Octadecylrhodamine B in vesicles. *J. Phys. Chem.* 91:3020–3023.

Klafter, J., and A. Blumen. 1984. Fractal behavior in trapping and reaction. *J. Chem. Phys.* 80:875–877.

Klafter, J., and A. Blumen. 1985. Direct energy transfer in restricted geometries. *J. Lumin.* 34:77–82.

Klausner, R. D., and D. E. Wolf. 1980. Selectivity of fluorescent lipid analogues for lipid domains. *Biochemistry.* 19:6199–6203.

Lakowicz, J. R. 1983. Principles of Fluorescence Spectroscopy. Plenum Press, New York.

Levitz, P., and J. M. Drake. 1987. Direct energy transfer in restricted geometries as a probe of the pore morphology of silica. *Phys. Rev. Lett.* 58:686–689.

Levitz, P., J. M. Drake, and J. Klafter. 1988. Critical evaluation of the application of direct energy transfer in probing the morphology of porous solids. *J. Chem. Phys.* 89:5224–5236.

Mabrey, S., and J. M. Sturtevant. 1976. Investigation of phase transitions of lipids and lipid mixtures by high sensitivity differential scanning calorimetry. *Proc. Natl. Acad. Sci. USA.* 73:3862–3866.

Maliwal, B. P., J. Kusba, J. R. Lakowicz. 1995. Fluorescence energy transfer in one dimension: frequency-domain fluorescence study of DNA-fluorophore complexes. *Biopolymers.* 35:245–255.

Marquardt, D. W. 1963. An algorithm for least-squares estimation of non-linear parameters. *J. Soc. Ind. Appl. Math.* 11:431–441.

Marsh, D. 1990. Handbook of Lipid Bilayers. CRC Press, Boca Raton, FL.

McClare, C. W. F. 1971. An accurate and convenient organic phosphorus assay. *Anal. Biochem.* 39:527–530.

Medhage, B., E. Mukhtar, B. Kalman, L. B.-Å. Johansson, and J. G. Molotkovsky. 1992. Electronic energy transfer in anisotropic systems. Part 5. Rhodamine-lipid derivatives in model membranes. *J. Chem. Soc. Faraday Trans.* 88:2845–2851.

Mendelsohn, R., G. L. Liang, H. L. Strauss, and R. G. Snyder. 1995. IR Spectroscopic determination of gel state miscibility in long-chain phosphatidylcholine mixtures. *Biophys. J.* 69:1987–1998.

O' Connor, D. V., and Philips, D. 1984. Time-Correlated Single Photon Counting. Academic Press, New York.

Ohta, N., T. Tamai, T. Kuroda, T. Yamazaki, Y. Nishimura, and I. Yamazaki. 1993. Direct trapping excitation energy transfer from rhodamine B to crystal violet in Langmuir-Blodgett monolayer and stacked multilayer films. *Chem. Phys.* 177:591–600.

Parasassi, T., M. DiStefano, M. Loiero, G. Ravaganan, and E. Gratton. 1994. Influence of cholesterol on phospholipid bilayers phase domains as detected by Laurdan fluorescence. *Biophys. J.* 66:120–132.

Pekcan, Ö., L. S. Egan, M. A. Winnik, and M. D. Croucher. 1990. Energy transfer in restricted dimensions: a new approach to latex morphology. *Macromolecules.* 23:2210–2216.

Prieto, M. J. E., M. Castanho, A. Coutinho, A. Ortiz, F. J. Aranda, and J. C. Gómez-Fernandez. 1994. Fluorescence study of a derivatized diacylglycerol incorporated in model membranes. *Chem. Phys. Lipids.* 69: 75–85.

Rojanski, D., D. Huppert, H. D. Bale, X. Dacai, P. W. Schmidt, D. Farin, A. Seri-Levy, and D. Avnir. 1986. Integrated fractal analysis of silica: adsorption, electronic energy transfer, and small-angle x-ray scattering. *Phys. Rev. Lett.* 56:2505–2508.

Sackmann, E. 1982. Physical foundations of the molecular organization and dynamics of membranes. *In* Biophysics. W. Hoppe, W. Lohmann, H. Markl, and H. Ziegler, editors. Springer-Verlag, Berlin. 425–457.

Sankaram, M. B., D. Marsh, and T. E. Thompson. 1992. Determination of fluid and gel domain sizes in two-component, two phase lipid bilayers. An ESR spin label study. *Biophys. J.* 63:340–349.

Sienicki, K., H. Itagaki, and W. L. Mattice. 1989. On the theory of concentration depolarization of fluorescence in one and two-component systems for multipole interactions in one, two and three dimensional medium. *J. Chem. Phys.* 91:4515–4521.

Snyder, B., and E. Freire. 1982. Fluorescence energy transfer in two dimensions. A numeric solution for random and non-random distributions. *Biophys. J.* 40:137–148.

Snyder, R. G., H. L. Strauss, and D. A. Cates, 1995. Detection and measurement of microaggregation in binary mixtures of esters and of phospholipid dispersions. *J. Phys. Chem.* 99:8432–8439.

Spink, C. H., M. D. Yeager, and G. W. Feigenson. 1990. Partitioning behavior of indocarbocyanine probes between coexisting gel and fluid phases in model membranes. *Biochim. Biophys. Acta.* 1023:25–33.

Tamai, N., T. Yamazaki, I. Yamazaki, A. Mizuma, and N. Mataga. 1987. Excitation energy transfer between dye molecules adsorbed on a vesicle surface. *J. Phys. Chem.* 91:3503–3508.

Valdes-Aguilera, O., and D. C. Neckers. 1989. Aggregation phenomena in xanthene dyes. *Acc. Chem. Res.* 22:171–177.

Van Der Meer, B. W., G. Coker III, and S.-Y. S. Chen. 1994. Resonance Energy Transfer. Theory and Data. VCH Publishers, Inc., New York.

Wolber, P. K., and B. S. Hudson. 1979. An analytical solution to the Förster energy transfer in two dimensions. *Biophys. J.* 28:197–210.

Yamazaki, I., N. Tamai, and T. Yamazaki. 1987. Picosecond fluorescence spectroscopy on excimer formation and excitation energy transfer of pyrene in Langmuir-Blodgett monolayer films. *J. Phys. Chem.* 91: 3572–3577.

Yang, C. L., P. Evesque, and M. A. El-Sayed. 1985. "Fractal-like", but nonfractal, behavior of one-step dipolar energy transfer on regular lattices with excluded volume. *J. Phys. Chem.* 89:3442–3444.